Sensors & Transducers, Vol. 0, Issue 0, Month 2016, pp. XX-YY

Sensors & Transducers

http://www.sensorsportal.com

A non-linear model for predicting tip position of a pliable robot arm segment using bending sensor data

[1] Elizabeth I. SKLAR, [2] Sina SAREH, [3] Emanuele L. SECCO, [1] Angela FARAGASSO and [1] Kaspar ALTHOEFER

[1] Department of Informatics, King's College London, Strand, London WC2R 2LS, UK
[2] Department of Aeronautics, Imperial College London, UK
[3] Dept of Mathematics & Computer Science, Liverpool Hope University, Liverpool, L16 9JD, UK
[1]*elizabeth.sklar,angela.faragasso,* kaspar.althoefer@kcl.ac.uk,
[2]s.sareh@imperial.ac.uk, [3]seccoe@hope.ac.uk

Received: Accepted: Published:

Abstract: Using pliable materials for the construction of robot bodies presents new and interesting challenges for the robotics community. Within the EU project entitled *STIFFness controllable Flexible & Learnable manipulator for surgical Operations (STIFF-FLOP)*, a bendable, segmented robot arm has been developed. The exterior of the arm is composed of a soft material (silicone), encasing an internal structure that contains air-chamber actuators and a variety of sensors for monitoring applied force, position and shape of the arm as it bends. Due to the physical characteristics of the arm, a proper model of robot kinematics and dynamics is difficult to infer from the sensor data. Here we propose a non-linear approach to predicting the robot arm posture, by training a feed-forward neural network with a structured series of pressures values applied to the arm's actuators. The model is developed across a set of seven different experiments. Because the STIFF-FLOP arm is intended for use in surgical procedures, traditional methods for position estimation (based on visual information or electromagnetic tracking) will not be possible to implement. Thus the ability to estimate pose based on data from a custom fiber-optic bending sensor and accompanying model is a valuable contribution. Results are presented which demonstrate the utility of our non-linear modelling approach across a range of data collection procedures.

Keywords: Bending sensing; pressure sensing; MR compatibility sensing; sensors for minimally invasive surgery; sensors for keyhole surgery; sensor fusion & interpretation; non-linear models

1. Introduction

Pliable manipulators represent a new branch of robotic construction that promises great potential, but is faced with intriguing challenges with respect to calibration and control (Althoefer *et al.*, 2014; Cianchetti *et al.*, 2014; Vogt *et al.*, 2013; Sareh *et al.*, 2014; Jiang *et al.*, 2012; Noh *et al.*, 2014). Traditional robot kinematics assume that a robot is constructed out of rigid material and that its body shape is fixed. Where there are joints, the body may bend—but not otherwise. If the body meets an object that is hard, there will be a collision in which the rules of rigid-body physics apply. However, when one of the colliding objects is not rigid, different rules apply. Indeed, within the computer graphics community,

much attention has been paid to the development of computational models of the behavior of soft bodies (e.g., Chadwick, Haumann & Parent, 1989). But such behaviors are new to the robotics community, since soft robot bodies composed of flexible materials have only recently been introduced.

Due to the unconventional characteristics of soft body robots, in order to properly and precisely model and control kinematics and dynamics, sensors must be employed strategically. Focusing on the estimation of *pose*, namely the position and orientation of the robot end-effector, different sensors have recently been proposed in the literature. Prominent examples include: off-the-shelf resistive flex sensors based on conductive ink, e.g., *FLXT*[1]; specific types of smart materials, e.g., *Ionic Polymer Metal Composite (IMPC)* (Punning *et al.*, 2007); soft sensors based on micro-channel of conductive liquid (eutecticGallium Indium, *eGaIn*); and sensors based on fiber optics. Resistive sensors based on conductive inks and IPMCs are bipolar devices and are not suitable for three-dimensional fabrication. The sensing systems based on eGaIn are attractive for integration in soft structures and robots; however, there is no data on biocompatibility of this material according to the datasheet published. Fiber optics are employed for curvature sensing in flexible robots. They function by sensing the change in optical characteristics of the light. These include optical sensors based on wavelength modulation (Patrick *et al.*, 1998; Allsop *et al.*, 2005), polarization (Feng *et al.*, 2011) and light intensity modulation (Liu *et al.*, 2010; Liu *et al.*, 2011; Noh *et al.*, 2015). From the electrical view, optical fibers are immune to magnetic field and electrical interference and, hence, a distinguished candidate for many industrial and medical applications. From the mechanical point of view, plastic optical fibers are very attractive for integration into soft structures due to their ability to follow the elastic deformation of the robot bodies in which they are embedded. Optical sensors based on *Fibre Bragg Grating* are costly and sensitive to temperature and strain (Yi *et al.*, 2010; Zhang *et al.*, 2007). Here, we employ light intensity modulation to produce a low-cost optical curvature sensor amenable for integration into for flexible, soft and extensible robotic arms.

The work presented here investigates the question of modelling the behavior of such a device, and here specifically studies a single-segment manipulator that has been developed within the EU project *STIFFness controllable Flexible & Learnable manipulator for surgical OPerations (STIFF-FLOP).* As described in Section 2, the device contains embedded air-chamber actuators and fiber-optic bending sensors. A series of experiments was conducted (detailed in Section 3) in which data was collected on the behavior of the actuators and the bending sensor, as well as a complementary set of additional sensors intended to provide "ground truth position" readings. Using the experimental data, a series of non-linear models of robot body-segment behavior were trained (described in Section 4). The results, presented in Section 5, indicate that the bending sensor, accompanied by our non-linear model, provides a reliable means of predicting pose, as measured against ground-truth position data.

In the work presented here, sensors and actuators are integrated together, inside the soft structure of the pliable arm, without any mechanical isolation. Here, the aim is to model sensor-actuator interactions. In related work, additional investigations have been conducted into solutions that minimize the negative aspects of the aforementioned interactions, because such interactions can contribute to noise; these are presented in Sareh *et al.*, 2015a and Sareh *et al.*, 2015b.

2. Hardware Description

A single segment of the STIFF-FLOP robot arm was used to perform the experiments described here. The segment is made of Ecoflex 00-50 Supersoft Silicone[2], with a chamber length of *30 mm* and diameter of *33 mm*. Figure 1 shows the segment in the experimental setup configuration.

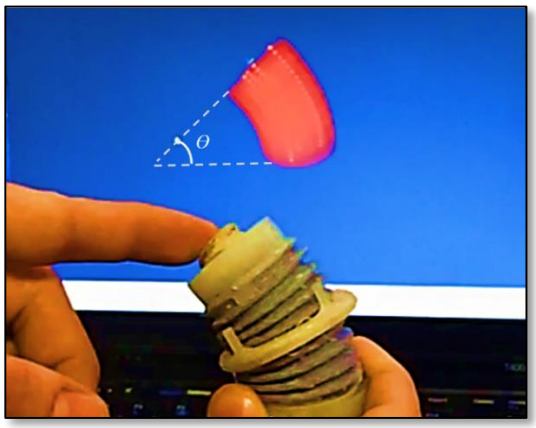

Fig. 1. A side view of the STIFF-FLOP robot arm segment with integrated fiber-optic bending and NDI Aurora position sensors, a pneumatic actuation system, and the estimated bending angle visualized in real-time.

2.1. Actuators

The segment incorporates three actuators - air chambers - which are equally distributed (every *120°*) around the circumference of a cross-section of the robot arm segment (see Figure 2a). These actuators support the moving, bending and extending of the arm.

The nature of the air-chamber actuators, combined with the material that the segment is made of, renders the whole manipulator *flexible.* It can easily bend from side to side, as well as compress and extend (like a spring). This means that the device will be inherently

[1] Flexpoint Sensor Systems, Inc., USA

[2] Smooth-On Inc., USA

safe for surgical procedures - the target task domain for the STIFF-FLOP project.

The air chambers are fed by *4 mm* diameter tubes, with air at a maximum pressure of *0.6 bar*. A set of three pressure regulators[3] supply air to the chambers, extracted from an external compressor upon triggering the actuator. Three analog signals, with a range of *1-10V*, are used to drive voltage regulators (Vr_1, Vr_2, Vr_3) in order to apply constant pressure (p_1, p_2, p_3) to each chamber of the device.

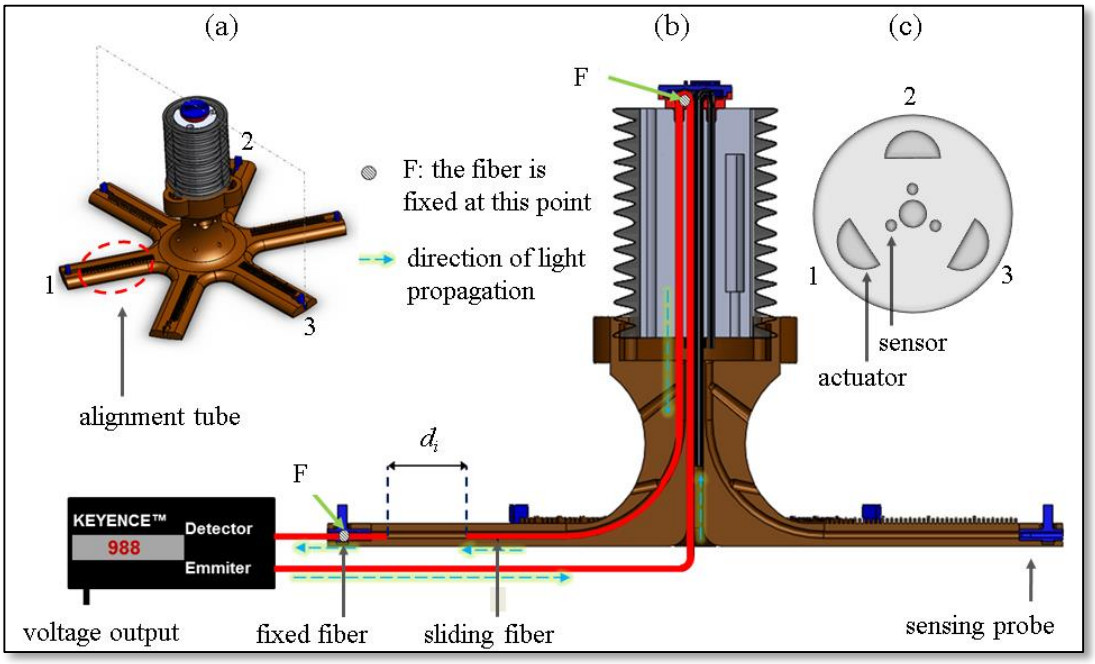

Fig. 2. (a) The overall structure of the STIFF-FLOP module with integrated bending sensor, (b) the configuration of fiber optic bending sensor, and (c) the cross section of the module indicating the position of pneumatic actuators and optical fiber

2.2. Bending sensors

The novel bending sensor is comprised of three pairs of optical fibers, also equally distributed around the central axis of the arm, as illustrated in Figure 2a. Each sensor is made of two optical fibers, which are connected to an emitter and a detector (Figure 2). The two fibers originate from a digital amplifier, a Keyence FS-N11MN Fiber Optic Sensor[4]. One fiber extends along the length of the arm segment, then bends at the top and returns to the base (as illustrated in Figure 2b). According to this setup, as soon as the manipulator moves, bends, extends or elongates, the corresponding lengths of the emitting fibers that are fitted inside the pliable arm change in response.

In other words, movement of the arm segment effects the distance, *d*, between the emitter and the detector, as indicated in Figure 2b, modulating the light intensity received by the fixed fiber at the opposite end of the sensor. This information is transduced into a voltage signal in the range of *1-5V*, by means of the aforementioned digital amplifier (Figure 2b). When the manipulator undergoes an amount of bending deformation in a particular orientation, a unique voltage matrix is generated:

$$Vs = (Vs_1\ Vs_2\ Vs_3)$$

2.3. Position sensors

An NDI Aurora System[5] was used to estimate the position and orientation of the robot arm, providing "ground truth" in order to measure the accuracy of the pose predicted by the Keyence-based bending sensors plus the non-linear model (described in Section 4). The Aurora sensor technology is based on electro-magnetic trackers, which allow real-time measurements of the position and orientation of each tracker (6 degrees of freedom). Four markers were used in the experiments described here: one on the manipulator base, one at the top and two on the side, located halfway along the length of the manipulator and held in place by means of a ring-shaped support

.

[3] SMC ITV0030
[4] Keyence Co., Ltd.
[5] AURORA 4 Port PM Tracking System V2, Northern Digital, Canada

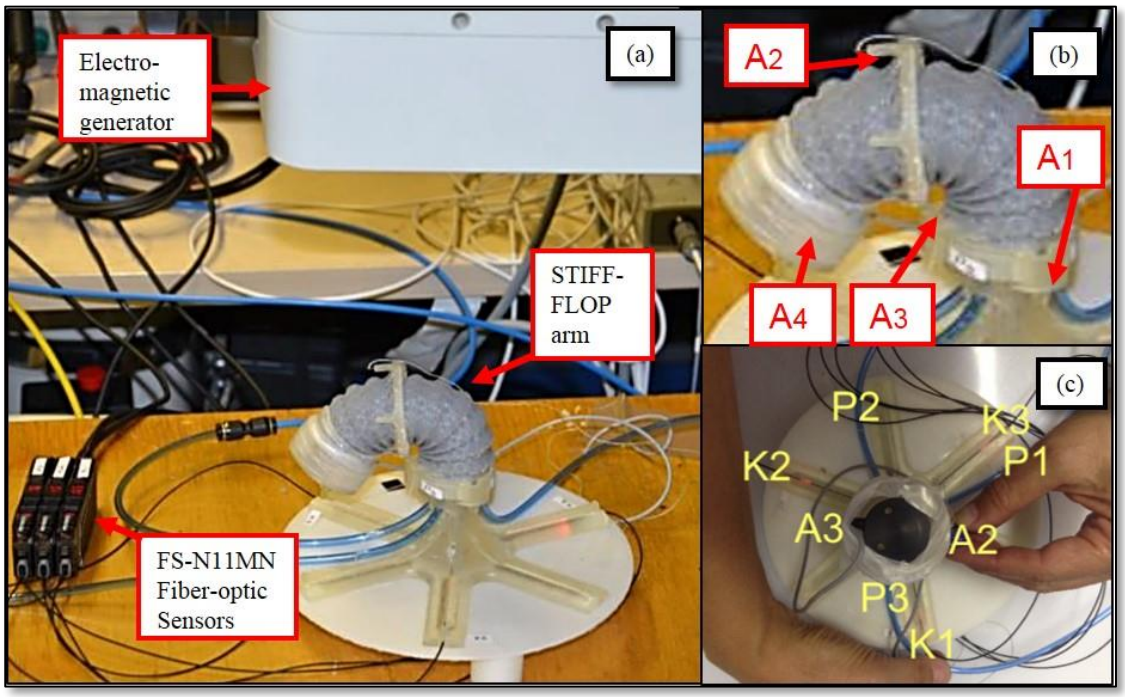

Fig. 3. (a) The experimental setup used for validation of the nonlinear bending model, (b) the location of NDI Aurora trackers $\{A_1, A_2, A_3, A_4\}$ embedded in the arm segment, and (b) the arrangement of fiber-optic sensors $\{K_1, K_2, K_3\}$.

The experimental setup is shown in Figure 3. The three Keyence sensors are labeled K_1, K_2 and K_3 (tiny red lights that can be seen on the base, within their housing). The two Aurora markers placed on the side of the segment are labeled A_2 (left side) and A_3 (right side). The other two Aurora markers are not labeled in the figure. The one on the base (A_1) is not visible because it was under the apparatus shown in the figure, within the center of the base, and the other was on the top (A_4), in the center of the circular black region in the middle of the figure. The three air-chamber actuators are labelled P_1, P_2 and P_3, and correspond to the positions where the thin blue tubing intersects with the arm segment.

3. Experiments

The goal of the experiments described here was to obtain data from the robot hardware and analyze that data to determine whether the position of the robot arm is predictable, given the data reported by the bending sensors. Since the ultimate goal is to develop this architecture into a multi-segmented flexible manipulator instrument to employ during keyhole surgery, we were interested to learn whether the Keyence sensor readings could be used as the basis of a model of the behavior of the robot arm. Thus, in a structured way (outlined below), we gathered data on the amount of pressure applied to the manipulator and the resulting positional data, as measured by the Keyence bending sensors, and also by the Aurora position sensors (for obtaining ground truth, against which we can compare the bending sensor data). In summary, our goal is to use the position sensor data to determine whether positioning information derived from the bending sensor is a good predictor of the amount of pressure applied to the manipulator.

3.1. Software and data acquisition architecture

The experimental setup involved two separate data acquisition systems, in order to collect bending sensor data independently from the ground truth position data. The first data acquisition system was designed to collect the bending sensor data in real-time. For this system, an interactive program was written in *LabVIEW*[6] and combined with an NI 6211 data acquisition card[7]. This program allows a user to control the applied pressure regulators (Section 2.1) and read data from the bending sensors (Section 2.2), at a sampling frequency of *22 Hz*. The second data acquisition system was designed to collect position sensor data in real-time (Section 2.3). For this system, a non-interactive program was written in ROS[8] and interfaced with the four Aurora markers described earlier. Data was collected from these sensors with a sampling frequency of *31 Hz*. This dual setup permits the recording and saving of measurements from two independent data collection systems, along with high-precision timestamps that allow synchronization between them. Collecting data independently ensures

[6] http://www.ni.com/labview/

[7] National Instruments, Ltd.

[8] Robot Operating System, http://www.ros.org

that there is no timing or processing noise coming from the (hopefully) redundant data collection system.

3.2. Protocol

We ran a series of seven experiments to collect data in a structured way, from the actuators, the bending sensors and the position sensors. Each of the three actuators, (P_1, P_2, P_3), could take on any of four values: *0.0, 0.2, 0.4* or *0.6 bar*, where *0.0 bar* is the *resting* state (where no pressure is applied). Our goal is to determine whether we can predict the position of the robot arm segment, given the pressure applied and the data collected from the bending sensor. As detailed in the next section, we developed a non-linear model that takes the three input pressure values and outputs the 3D pose of the arm segment.

Our experiments were designed to address two primary research questions. *First*, the overarching question was whether we could build a model (either linear or non-linear) with which to predict the arm pose from the bending sensor data. *Second*, due to the nature of the air-pressure actuators, we hypothesized that air could accumulate in the chambers and so the sequence of actuator commands would be important in developing our model; i.e., the pressure applied at a single instant in time, *t*, might not be reliable enough on its own to predict position - it might be necessary to model a set of {*t…t-n}* pressure values in order to produce an accurate prediction of robot arm position. To address this second question specifically, we designed experiments in two groups, as described next.

The first group of experiments (1-4) was designed to evaluate the bending sensor performance when varying amounts of pressure were applied to the air-chamber actuators. Four sequences of combinations of pressure values were applied to the chambers. In each case, the device started from a resting state. After applying each pressure-value combination, data was collected for *10 seconds* in order to give the manipulator and the sensors time to settle and reach a steady state. After applying each combination in the designated sequence for each of these four experiments, the pressure values were reset to *0.0*, allowing the manipulator to return to its resting position (i.e., all the three air chambers empty). The sequences of pressure values were computed according to the pseudo-code in Figure 4, where the constant, P_1, was set as shown in Table 1.

The second group of experiments (5-7) were designed to evaluate the bending sensor performance when accumulating amounts of pressure were applied to the air-chamber actuators. Here, the pressure was continually increased, without allowing the manipulator to return to its resting position in between pressure combinations in each sequence. Figure 5 contains the pseudo-code for experiment 5. Experiments 6 and 7 followed the sequences listed in Table 2, with a 10-second wait before moving to the next set of values.

```
P1 = constant
for P2 in {0.0, 0.2, 0.4, 0.6}:
  for P3 in {0.0, 0.2, 0.4, 0.6}:
    apply {P1,P2,P3}
    wait 10 sec
    apply {0.0, 0.0, 0.0}
    wait 10 sec
```

Fig. 4. Pseudo-code for sequences used in experiments 1-4 (pressure values in bar).

Table 1. Values of P1 for experiments 1-4.

experiment	value of P_1
1	*0.0*
2	*0.2*
3	*0.4*
4	*0.6*

The distinction between the two groups of experiments - variation (experiments 1-4) versus accumulation (experiments 5-7) of actuator pressure - is illustrated in Figures 7c and 8c. Figure 7c shows the applied pressure values, over time, for experiment 3, where the air chambers were allowed to empty and return to the resting state in between consecutive applications of pressure. In contrast, Figure 8c shows the applied pressure values for experiment 6, where the air chambers were not emptied in between consecutive applications of pressure; these sequences were designed to determine whether an accumulation of air inside the chambers impacted the values returned by the bending sensors.

```
{P1, P2} = {0.0, 0.0}
for P3 in {0.0, 0.2, 0.4, 0.6}:
  apply {P1, P2, P3}
  wait 10 sec
{P1, P3} = {0.0, 0.0}
for P2 in {0.0, 0.2, 0.4, 0.6}:
  apply {P1, P2, P3}
  wait 10 sec
{P2, P3} = {0.0, 0.0}
for P1 in {0.0, 0.2, 0.4, 0.6}:
  apply {P1, P2, P3}
  wait 10 sec
```

Fig. 5. Pseudo-code for sequences used in experiment 5 (pressure values in bar).

Table 2. Sequences used in experiments 6 and 7: pressure values in bar, (P_1, P_2, P_3).

experiment 6	experiment 7
(0.0, 0.0, 0.0)	*(0.0, 0.0, 0.0)*
(0.0, 0.0, 0.2)	*(0.0, 0.2, 0.0)*
(0.0, 0.2, 0.2)	*(0.2, 0.2, 0.0)*
(0.2, 0.2, 0.2)	*(0.2, 0.2, 0.2)*
(0.2, 0.2, 0.4)	*(0.2, 0.4, 0.2)*
(0.2, 0.4, 0.4)	*(0.4, 0.4, 0.2)*
(0.4, 0.4, 0.4)	*(0.4, 0.4, 0.4)*
(0.4, 0.4, 0.6)	*(0.4, 0.6, 0.4)*
(0.4, 0.6, 0.6)	*(0.6, 0.6, 0.4)*
(0.6, 0.6, 0.6)	*(0.6, 0.6, 0.6)*
(0.0, 0.0, 0.0)	*(0.0, 0.0, 0.0)*

3.3. Raw data analysis

The raw data was noisy, which is not unexpected. For example, large spikes occurred occasionally in the Aurora sensor readings. As a result, we introduced a *filtering* process in which we computed the average of the actuator and sensor values over a 5-sample window. This process successfully smoothed out any anomalies and other noise from the raw data. Table 3 shows the number of samples of raw data collected in each experiment and the number of samples from each experiment after the filtering process was performed.

Table 3. Number of samples used for training.

experiment	*raw data*	*filtered*
1	9333	1866
2	8706	1741
3	8028	1605
4	8244	1648
5	3688	737
6	2758	551
7	2680	535
total	*43437*	*9813*

The raw data values for the ground-truth position are meaningless within an absolute reference frame—we are really interested in the *change* in position over time. Thus we use the *displacement* values for both position and bending sensor data. This has the added benefit of allowing us to ignore any fixed calibration bias in either type of sensor. The displacement of the bending sensor values, from the starting (resting) position, over time, is computed as:

$$disp_i = V_i - V_0$$

where V_i is the current position (at time i) and V_0 is the starting (resting) position. Note that the bending sensor displacement values can be negative. The displacement, or *distance moved*, for each of the Aurora markers, is measured from the starting position using the Euclidean distance:

$$dist_i = \sqrt{[(x_i - x_0)^2 + (y_i - y_0)^2 + (z_i - z_0)^2]}$$

Figures 7 and 8 display examples of the filtered data collected during two of the experiments (numbers 3 and 6, respectively). The top plot (a) in each figure shows the displacement of the bending sensor values. The middle plot (b) shows the distance for each of the Aurora markers, measured from their starting position, also over time. The bottom plot (c) shows the corresponding applied pressure values, over the same timescale. It is easy to see that as different amounts of pressure were applied via the air-chamber actuators, the displacement of the bending sensors changed, as did the displacement distance for the position markers.

Our first research question asks whether the bending sensor values can reliably predict the position of the robot arm segment. Obviously, if there is a linear correlation between these values, our job would be easy. Unfortunately, this is not the case. Our next step is to investigate construction of a non-linear model to reach our goal, as described in Section 4, below.

4. Model

Our overall aim is to construct a computational model that will reliably predict the position of the arm segment, based on sensor data. After collecting the experimental data described above, we then designed four different models, varying the inputs and outputs, to determine empirically which properties of the arm can be measured in real-time and produce reliably predictable results. All of the models are based on *feed-forward neural networks* (Mcculloch & Pitts, 1943; Hinton, 1989; Pomerleau, 1992). They are trained using *back-propagation* (Rumelhart, Hinton & Williams, 1986), with a learning rate of *0.001* and momentum set to *0.9*.

Table 4 contains the parameters that define the architecture of each neural network model. The first two rows in the table are designed to predict the applied pressure values, given bending sensor values and position values as input (models ***nnk*** and ***nna***, respectively). The second two rows are designed to predict the position values, given the applied pressure and bending sensor values as input (models ***nnar*** and ***nnp***, respectively). The last row represents what we set out to do: predict the position values, given the bending sensor values. However, we cannot achieve this overall aim if we do not have reliable models for each of the different dynamic properties of the arm, i.e., the applied pressure values, the position sensor values and the bending sensor values. More discussion of this appears in Section 5.

For the applied pressure, three values are considered, (P_1, P_2, P_3), in bar, for each of the three air-chamber actuators (Section 2.1). For the bending sensor, three values are considered, (K_1, K_2, K_3), in volts, for each of the three fiber-optic bending sensors (Section 2.2). For the position sensor, twelve values are considered, (x, y, z), location in 3D space for each of the four position markers (Section 2.3).

Table 4. Parameters for neural networks trained.

nnet type	*input source*	*num. input nodes*	*num. hidden nodes*	*output target*	*num. output nodes*
nnk	*bending*	3	4	*pressure*	3
nna	*position*	12	8	*pressure*	3
nnar	*pressure*	3	8	*position*	12
nnp	*bending*	3	8	*position*	12

The networks were each trained in *rounds*, using *7*-fold cross validation and 500,000[9] generations per round, using data from all seven experiments. The network weights were all initialized randomly. The

[9] The ***nnp*** network was trained over 100,000 generations per round.

rounds proceeded as follows. The first training round was executed on the data for experiment 1. Then the results were evaluated on each of the remaining 6 experimental data sets (experiments 1-6). For the second training round, each network's weights were initialized to the weights of the best-performing network from the previous round (a process based on *simulated annealing*), and again, the network was evaluated against the remaining 6 experimental data sets. In other words, in the second round, the training data set was from experiment 2, and the evaluation data was the combined set of data from experiments 1 plus 3-7.

5. Results

The results from training the models are shown in Table 5. The values in the table are the best error rate for each of the four networks trained. The lowest training error occurred with networks ***nnar*** and ***nnp***. Table 6 shows the average error rate for each of the networks across the evaluation data set (i.e., the other 6 experiment data files). The lowest absolute evaluation error occurred with the same two networks (***nnar*** and ***nnp***).

Table 5. Error rates from training.

training set	***nnk***	***nna***	***nnar***	***nnp***
1	0.077	0.122	0.004	**0.002**
2	0.089	0.140	0.003	**0.002**
3	0.095	0.132	0.004	**0.002**
4	0.133	0.172	0.008	0.003
5	0.088	0.109	0.004	0.005
6	0.075	0.080	**0.002**	0.003
7	0.077	0.083	0.003	0.003
overall	*0.091*	*0.120*	***0.004***	***0.003***

Table 6. Error rates from evaluation.

training set	***nnk***	***nna***	***nnar***	***nnp***
1	0.469	0.282	0.027	0.037
2	0.270	0.259	0.011	0.013
3	0.253	0.295	0.012	0.013
4	0.394	0.219	0.022	0.012
5	0.274	0.222	0.012	0.059
6	0.234	0.353	0.012	0.028
7	0.370	0.313	0.020	0.068
overall	*0.323*	*0.278*	***0.016***	***0.033***

Figure 6 illustrates the improvement in error rate during training. The values plotted are the mean error every 1000 generations. Results from two different experiments are shown (3 and 6), for comparison. Note the different ranges on the *y*-axes for each row of plots. This is because the pairs of networks are predicting different outputs (pressure or position values). In all cases, the shape of the training error is as expected: the networks learn quickly in the early generations and then level out, and improvement tails off in later generations.

As mentioned earlier, our goal is to model the relationships between the actuator and sensor data collected during our experiments. We want to be able to predict the position of the arm segment, given bending sensor data. This could either be done directly, with bending sensor values as inputs to our model and position values as output (i.e., network ***nnp***); or it could be done directly, with bending sensor data used to predict pressure values, and then predicted pressure used to predict position (i.e., network ***nnk*** followed by ***nnar***). Either method is a reasonable approach, albeit the latter method is more computationally expensive and more prone to error. Looking at the training results in Tables 5 and 6, it is clear that predicting position is more accurate than predicting bending sensor values. *These results answer our first research question: it is possible to build a model (non-linear) which with we can accurately predict position from bending sensor data.*

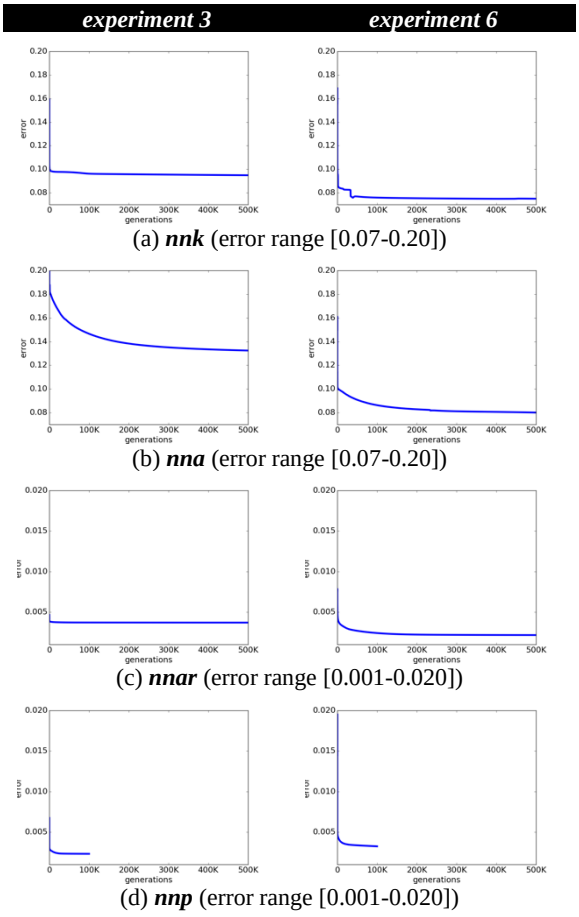

Fig. 6. Improvement in error during training. The *x*-axis starts at 0 and extends for 500K generations (except in the case of the ***nnp*** model, where training was completed after 100K generations). The *y*-axis contains the error rate, as labelled. See text for details.

One additional point to make is that the training results did not vary across the different experiments, meaning that the sequence of actuator commands applied to the arm segment do not impact the model. *This answers our second research question.* We had hypothesized that the results would be different when

we returned the arm segment to its resting position in between each new set of applied pressure values (experiments 1-4), as opposed to accumulating the pressure (experiments 5-7). *However, the differences in training between the two groups of experiments is negligible.*

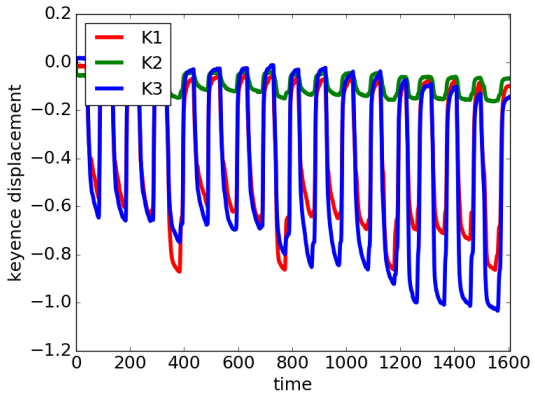

(a) displacement of Keyence sensor values

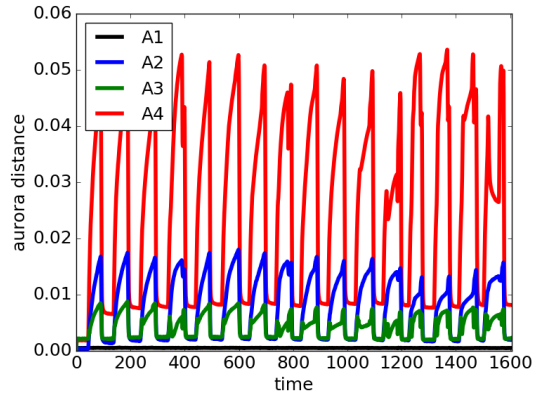

(b) displacement distance of Aurora markers

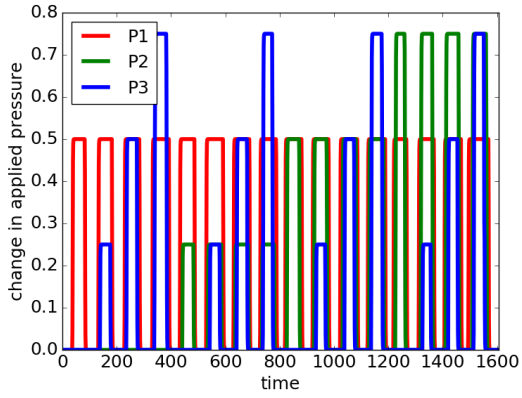

(c) applied pressure

Fig. 7. Filtered data from experiment 3, over time (*x*-axis). See text for explanation.

6. Summary

We have described a non-linear method for modelling the position of a flexible robot arm segment, using a novel fiber-optic bending sensor and a feed-forward neural network model. In a series of 7 experiments, we collected actuator and sensor data, including ground truth position information, in the attempt to construct a reliable model for how the arm segment moves as a result of different actuator commands being applied to the device. We experimented with four different neural network architectures to learn a model of the arm's behavior.

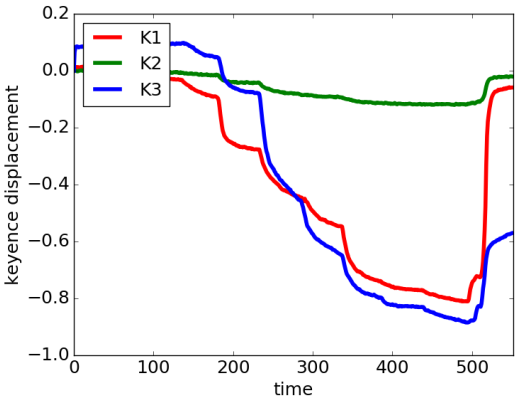

(a) displacement of Keyence sensor values

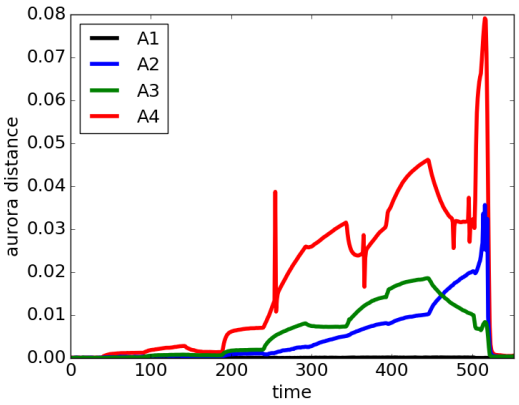

(b) displacement distance of Aurora markers

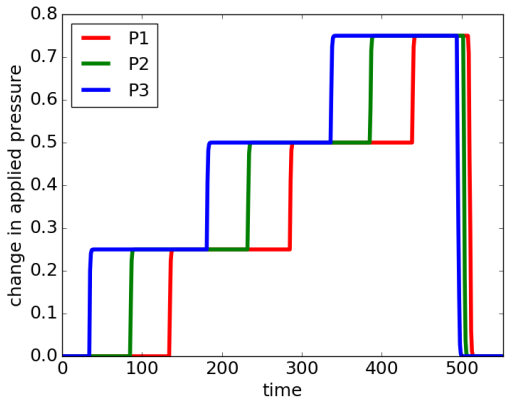

(c) applied pressure

Fig. 8. Filtered data from experiment 6, over time (*x*-axis). See text for explanation.

Our results show that the neural network model produces a reliable estimate for the pose of the arm segment. In addition, we have demonstrated that the model is invariant to the order in which actuator commands are applied. This is an important result. Prior to conducting these experiments, we had been concerned about the accumulative effect of the type of air-chamber pressure actuators employed in the arm segment. Now we know that the neural network model can estimate pose regardless of recent arm movements leading up to the point of estimation.

The next steps with this work involve applying the model in a more dynamic way, rather than the

structured sequences of "move-and-wait" commands tested here.

Acknowledgements

The research leading to these results has received funding from the European Commission's Seventh Framework Programme; project STIFF-FLOP (Grant No: 287728). This work was also supported by a US-UK Fulbright-King's College London Scholar Award, and a University of Liverpool Research Fellowship.

References

T. Allsop, M., Dubov, A. Martinez, F. Floreani, I. Khrushchev, D. Webb and I. Bennion (2005), Long period grating directional bend sensor based on asymmetric index modification of cladding, *Electronics Letters*, 41(2).

K. Althoefer, F. Iida, T. Nanayakkara, H. Liu, E. L. Secco, and H. A. Würdemann (2014), Workshop on Soft and Stiffness-Controllable Robots for Minimally Invasive Surgery, *IEEE International Conference on Robotics and Automation (ICRA)*.

J. E. Chadwick, D. R. Haumann and R. E. Parent (1989), Layered Construction for Deformable Animated Characters, *Computer Graphics, 23(3).*

M. Cianchetti, T. Ranzani, G. T., Gerboni, T. Nanayakkara, K. Althoefer, P. Dasgupta and A. Menciassi (2014), Soft Robotics Technologies to Address Shortcomings in Today's Minimally Invasive Surgery: The STIFF-FLOP Approach, *Soft Robotics. 1(2),* pp. 122-131.

G. E. Hinton (1989), Connectionist learning procedures, *Artificial Intelligence, 40(1-3)*, pp. 185-234.

A. Jiang, G. Xynogalas, P. Dasgupta, K. Althoefer and T. Nanayakkara (2012), Design of a variable stiffness flexible manipulator with composite granular jamming and membrane coupling, *IEEE/RSJ International Conference on Intelligent Robots and Systems (IROS)*, pp. 2922–2927.

H. Liu, J. Li, X. Song, L. D. Seneviratne and K. Althoefer (2011), Rolling Indentation Probe for Tissue Abnormality Identification During Minimally Invasive Surgery, *IEEE Transactions on Robotics, 27(3),* pp. 450-460.

H. Liu, D. P. Noonan, B. J. Challacombe, P. Dasgupta, L. D. Seneviratne and K. Althoefer (2010), Rolling mechanical imaging for tissue abnormality localization during minimally invasive surgery. *IEEE Transactions on Biomedical Engineering, 57(2),* pp. 404-414.

W. S. McCulloch and W. Pitts (1943), A logical calculus of the ideas immanent in nervous activity, *Bulletin of Mathematical Biophysics* 5, pp. 115-133.

Y. Noh, S. Sareh, H. A. Würdemann, H. Liu, J. Housden, K. Rhode and K. Althoefer (2015), Three-axis Fibre-optic Body Force Sensor for Flexible Manipulators, *IEEE Sensors Journal, 16(6),* pp. 1641-1651.

Y. Noh, S. Sareh, J. Back, H. Würdemann, T. Ranzani, E. L. Secco, A. Faragasso, H. Liu and K. Althoefer (2014), A Three-Axial Body Force Sensor for Flexible Manipulators, *IEEE International Conference on Robotics & Automation (ICRA),* pp. 6388-6393.

Y. Noh, E. L. Secco, S. Sareh, H. Würdemann, A. Faragasso, J. Back, H. Liu, E. I. Sklar and K. Althoefer (2014), A Continuum Body Force Sensor Designed for Flexible Surgical Robotic Devices, *International Conference of the IEEE Engineering in Medicine and Biology Society (EMBC).*

H. Patrick, C. Chang and S. Vohra (1998), Long period fibre gratings for structural bend sensing, *Electronics Letters, 34(18),* pp. 1773-1775.

D. Pomerleau (1992), *Neural Network Perception for Mobile Robot Guidance*, Ph.D. dissertation, Carnegie Mellon University, Pittsburgh, USA.

A. Punning, M. Kruusmaa and A. Aabloo (2007), Surface resistance experiments with IPMC sensors and actuators, *Sensors and Actuators, A: Physical, 133*.

J. Feng, Y. Zhao, X.-W. Lin, W. Hu, F. Xu and Y. Q. Lu (2011), A Transflective Nano-Wire Grid Polarizer Based Fibre-Optic Sensor, *Sensors, 11(3)*, pp. 2488–2495.

D. E. Rumelhart, G. E. Hinton and R. J. Williams (1986), Learning representations by back-propagating errors, *Nature, 323*.

S. Sareh, A. Jiang, A. Faragasso, Y. Noh, T. Nanayakkara, P. Dasgupta, L. Seneviratne, H. Würdemann and K. Althoefer (2014), Bio-Inspired Tactile Sensor Sleeve for Surgical Soft Manipulators, *IEEE International Conference on Robotics Automation (ICRA*), pp. 1454-1459.

S. Sareh. Y. Noh, T. Ranzani, H. Würdemann, H. Liu and K. Althoefer (2015a), A 7.5 mm Steiner chain fibre-optic system for multi-segment flex sensing, *IEEE/RSJ International Conference on Intelligent Robots and Systems (IROS).*

S. Sareh, Y. Noh, M. Li, T. Ranzani, H. Liu and K. Althoefer (2015b), Macrobend optical sensing for pose measurement in soft robot arms, *Smart Materials and Structures, 24 (12),* article 125024.

E. L. Secco, Y. Noh, S. Sareh, H. A. Würdemann, H. Liu and K. Althoefer (2014). Modular integration of a 3 DoF F/T sensor for robotic manipulators, *4th Joint Workshop on Computer/Robot Assisted Surgery (CRAS)*, pp. 125-126.

D. M. Vogt, Y. L. Park and R. J. Wood (2013), Design and Characterization of a Soft Multi-Axis Force Sensor Using Embedded Microfluidic Channels, *IEEE Sensors Journal, 13(10).*

I. B. Wanninayake, E. L. Secco, L. D. Seneviratne and K. Althoefer (2013), A Novel Probe Designed to Estimate Soft Tissue Stiffness in MIS, Workshop on Cognitive Surgical Robotics, *International Conference on Intelligent Robots and Systems* (IROS).

H. Würdemann, E. L. Secco, T. Nanayakkara, K. Althoefer, K. Lis, L. Mucha, K. Rohr and Z. Nawrat (2013). Mapping Tactile Information of a Soft Manipulator to a Haptic Sleeve in RMIS, *3rd Joint Workshop on New Technologies for Computer/Robot Assisted Surgery (CRAS)*.

J. Yi, X. Zhu, L. Shen, B. Sun and L. Jiang (2010), An Orthogonal Curvature Fibre Bragg Grating Sensor Array for Shape Reconstruction, *Communications in Computer and Information Science, 97,* pp 25-31.

X. Zhang, J. J. Max, X. Jiang, L. Yu and H. Kassi (2007), Experimental investigation on optical spectral deformation of embedded FBG sensors, *Proceedings of SPIE 6478, Photonics Packaging, Integration, and Interconnects VII,* article 647808.